Octree-Based Mascon Model for Small Body Gravity Fields

Article *in* Journal of Guidance, Control, and Dynamics · July 2019

DOI: 10.2514/1.G004008

2 authors:

Arunkumar Rathinam
University of Luxembourg
28 PUBLICATIONS **70** CITATIONS
SEE PROFILE

Andrew G Dempster
UNSW Sydney
487 PUBLICATIONS **9,463** CITATIONS
SEE PROFILE

An Octree-based Mascon model for Small Body Gravity Fields

Arunkumar Rathinam* and Andrew G. Dempster†
University of New South Wales, Sydney, NSW, 2052, Australia

Nomenclature

G	=	Gravitational constant ($6.67408 \times 10^{-11}\ m^3 kg^{-1} s^{-2}$)
μ_g	=	Standard gravitational parameter ($m^3 s^{-2}$)
r_i	=	distance from i^{th} octree node's centroid to external point (m)
N	=	Number of octree nodes
U	=	Gravitational potential $\in \mathbb{R}^1$
∇U	=	Gravitational acceleration $\in \mathbb{R}^{3\times1}$
$\nabla\nabla U$	=	Gravity gradient matrix *or* Hessian of the potential $\in \mathbb{R}^{3\times3}$
$\mathbf{r_i}$	=	Vector from variable field point to polyhedron vertex
$\mathbf{E_e}$	=	Edge dyad $\in \mathbb{R}^{3\times3}$
$\mathbf{F_f}$	=	Face dyad $\in \mathbb{R}^{3\times3}$
L_e	=	Factor per-edge $\in \mathbb{R}^1$
ω_f	=	Factor per-face $\in \mathbb{R}^1$
m	=	Mass (kg)
ρ	=	Density (kgm^{-3})
V	=	Volume (m^3)
μ	=	mean
σ	=	standard deviation

I. Introduction

Small celestial bodies are topics of research interest in different fields such as scientific exploration, planetary defense and space resource utilization. Exploration missions ([1–3]) performed in-situ science experiments on the small bodies to characterize the minerals and their composition to help our understanding of the formation of the solar system. Recent sample return missions Hayabusa-2 [4] to Ryugu (C-type asteroid) and Osiris-REX [5] to Bennu (B-type asteroid) are expected to provide additional knowledge on the evolution of the planets, especially the origin of water

*PhD student, Australian Centre for Space Engineering Research, UNSW Electrical Engineering and Telecommunications; a.rathinam@unsw.edu.au
†Professor, Australian Centre for Space Engineering Research, UNSW Electrical Engineering and Telecommunications; a.dempster@unsw.edu.au

and organic matter. Planetary defense research analyzes the potential threats to Earth posed by the small bodies and works on developing technologies to mitigate them [6]. To date, small body exploration missions have been restricted to rendezvous, in-situ experiments, and sample-return missions. Future missions will target the mineral-rich asteroids towards resource extraction and utilization to boost space exploration activities ([7, 8]).

With an increase in the number of missions, the level of autonomy is expected to increase in future missions. To operate autonomously in the proximity of a small celestial body, the spacecraft must have a good knowledge of the orbital dynamics and this helps the on-board state estimation algorithms to better estimate the spacecraft and asteroid states. To study the orbital dynamics, a good estimate of the gravitational field around the bodies is essential. A small body's irregular shape accompanied with non-uniform mass distribution can make it difficult to model the gravitational field around the bodies in a more general form. There are different established methods available in the literature to calculate the gravitational potential of a non-spherical body. The classical representation is *spherical harmonic expansion* ([9, 10]), which expands the gravity potential into a harmonic series of finite order depending on the accuracy needed and explicitly computes the series coefficients. Spherical harmonics are guaranteed to converge to the correct gravity field outside of a circumscribing sphere but are always considered to be an approximation due to series truncation and that it provides no information about a field point either inside or outside of the body [11]. Another well-known approach is the *polyhedron method* [11], where a constant density polyhedron that precisely represents the shape of an object using planar faces, edges and vertices is used. The expressions were derived for the gravitational potential, acceleration and Hessian of a homogeneous polyhedron using the dyads of second-order are presented in [11] and the computed values are definite for the given shape and density. An exact solution of gravitational forces can be computed using the polyhedron method and the expressions were derived for the gravitational potential, acceleration and Hessian of a homogeneous polyhedron using the dyads of second-order [11]. This approach requires significantly larger computational effort to compute the gravitational potential and its derivatives. A third approach is the *mascons approach* (also known as *mascons*), where a body of given shape is approximated by a set of point masses (mascons) placed in a suitable way to reproduce the body's mass distribution [12]. Although this method is easier to develop, it has several deficiencies due to replacing the true body's continuous mass distribution with a field derived from spheres with modified density values based on the packing fraction [13]. The analysis of results of mascon models with different packing fraction as well as their limits are discussed in [14]. In another mascon-based approach presented in [13], a polyhedron shaped source is divided into tetrahedrons by joining each triangular face to the center of the asteroid. The centroid of each tetrahedron is determined and considered as a mascon source for the calculation of gravitational potential and its derivatives. The gravitational potential of irregular bodies using a non-uniform mascon distribution derived from unstructured volume meshes was studied in [15]. To improve the computational efficiency of mascon models and its usage in low altitudes, the performance of different packing arrangements of mascon elements inside the mascon model was investigated in [16]. The combination of spherical harmonic and the mascon model was also studied

in [16] and the results suggest that it offer similar accuracy compared to homogeneous mascon model but with smaller memory footprints.

In this work, we present a new mascon-based approach to compute the gravity potential and its derivatives using an octree model of an irregular small celestial body. An octree efficiently represents the 3D space using a tree data structure where each node has exactly eight children and is recursively divided until a predefined condition is satisfied. Octree modeling can be applied to both low and high fidelity models and it can be scaled to greater accuracy depending on the computation requirement. The basics of octrees is discussed in section II.A, and modeling techniques such as variable-depth and uniform-depth are discussed in section II.B. The uniform octree model presented in this work is the same as a grid of mascons presented in earlier works [11], [14], [16]. The novelty of the work lies in the Variable-octree methods and the octree construction approach. Using the point cloud data and the octree approach, the outer occupied nodes can be classified directly, but to select inner nodes that are enclosed, a section and boundary approach is presented in section II.C. Section III discusses the calculation of the gravity potential and its derivatives using a mascon approach. The details of the numerical simulation including the asteroid models and two specific cases are discussed in section IV. The results of the simulation including the variable-depth octree approach, uniform-depth octree approach and polyhedron approach are presented in section V along with the plots for gravity potential and surface gravity for both cases. Finally the discussions conclude in section VI.

II. Octree modeling of an irregular body

A. Octree

An octree is a hierarchical tree data structure, often used to partition three-dimensional space. Similar to using an N-dimensional binary tree (2^N-ary tree) to represent an N-dimensional object ([17, 18]), an octree (2^3 or octary tree) is used to represent a three-dimensional object. The *root node* of an octree represents the smallest cube that encloses the object. Each node in an octree is either *an internal node* (a node with eight children) or *a leaf node* (a node without children); a leaf node is also known as *a bin* or *a voxel*. A representation of an Octree-based partitioning of 3D space is shown in fig. 1. In general an octree of an object is constructed using the object's point cloud as a base. The root node of an octree represents the 3D volume that encloses the point cloud of an object. The root node is then divided recursively until each leaf node satisfies the predefined conditions. The major parameters for octree division include *octree depth or level*, *leaf node dimensions* and *the number of points inside a leaf node*. The parameters are used individually or in combinations during octree construction depending upon the modeling approach. The depth of an octree indirectly constraints the node dimensions. The outer dimensions of the asteroid provide a rectangular cuboid, however previous studies [11], [14] used spherical packing inside a cube for mascon based gravity field computation. By equaling all the root node dimensions to the maximum length of the asteroid dimensions one can construct the cube-shaped octree nodes.

In this case, the root node volume is significantly larger, but this additional volume will be removed during the octree construction process and does not affect other steps after octree construction. The node dimensions (pre-defined or required) at specified level can be achieved by changing the octree root node dimensions accodingly. The centroid of the root node is also matched with the polyhedron's centroid; this ensures the octrees are uniformly divided and mascons are places around the center. The root node is considered as level-0 (higher level), when it is divided to the next level, the dimensions of each child node are half of the parent node. For example, at level-2 (lower level), the node dimensions are $(\frac{1}{4})^{th}$ of root node dimensions and at level-5 (lower level), the node dimensions are $(\frac{1}{2^5} = \frac{1}{32})$ of root node dimensions.

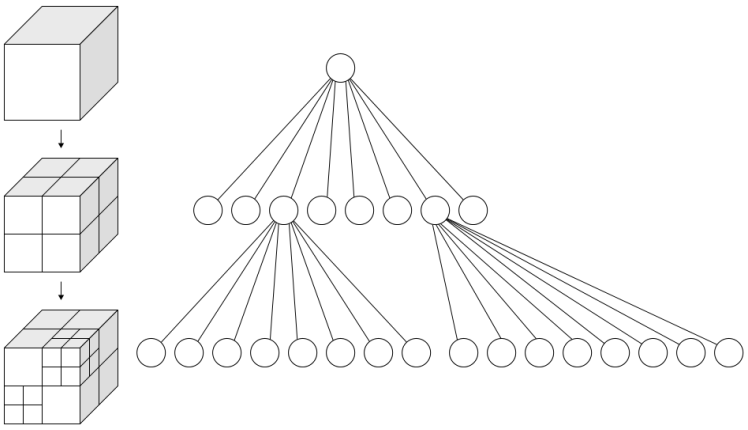

Fig. 1 Recursive subdivision of a 3D volume into octants and their corresponding octree [19]

B. Modeling methods

The asteroid's shape model contains the list of vertices and faces, the vertices location is used as the point cloud to build the octree model.

1. Uniform depth

In this method, the root node of an octree is recursively divided until all the leaf nodes reach the desired octree depth. During recursive division, the nodes are divided irrespective of whether a node is occupied by point(s) or not. Once the nodes are divided, for each point in the point cloud a corresponding leaf node is identified through validating the point's location against the leaf node boundary coordinates. Since the vertices of the shape model are used as the point cloud, the list of nodes occupied by the points provide the leaf nodes located at the outer layer of an octree. It does not provide any information on the inner nodes that constitute the entire volume of the octree. To identify all the leaf nodes (including enclosed inner nodes) that contribute to the volume of the model, section II.C discusses the enclosed node selection process. This node selection process is common for both octree modeling methods presented in this work.

2. Variable depth

In variable-depth octree modeling method, a root node of an octree that encloses all the points is divided into eight child nodes. Each child node is validated for two conditions, first, the point(s) occupancy. And if the leaf node is occupied, then it is validated against the minimum level node depth (for lower levels). The child node is divided into the next level node only if a node is occupied by point(s) and the node depth is below required octree depth. This process repeats until every octree leaf node satisfy the specified conditions. If a child node is empty, then it will be classified as a leaf node, even if the node is located at higher octree level (larger node size).

In the variable-depth octree model, the leaf nodes are distributed across multiple levels and the node dimensions vary accordingly. Within the octree model, higher level nodes have larger volume and usually found at the center of the constructed octree model. Whereas, the nodes in a lower octree level constitute the outer nodes and are smaller in size compared to the nodes in lower octree levels. The variable-depth octree division method is more efficient than the uniform-depth method because it allows dividing the model into smaller node sizes without compromising the computation requirements. Like the uniform-depth model, the octree model generated contains the list of outer leaf nodes and the enclosed nodes will be found as described in the following section. The point cloud data of asteroid Itokawa along with the cross-sections of both the octree models are shown in fig. 2.

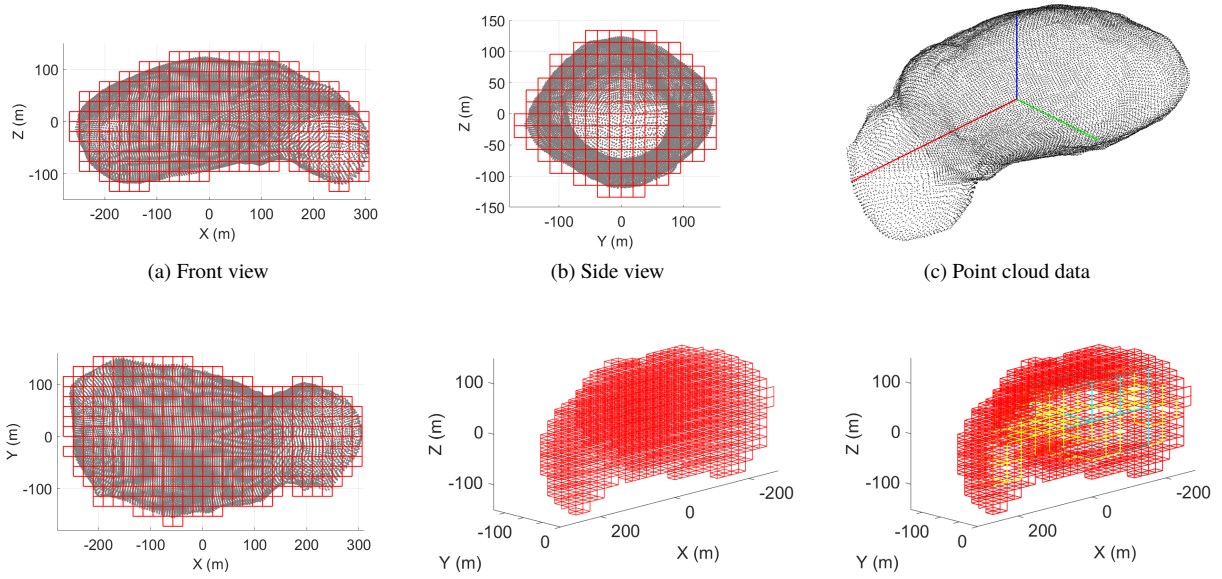

(a) Front view

(b) Side view

(c) Point cloud data

(d) Top view

(e) Section of a uniform depth octree model with leaf nodes at level-5

(f) Section of a variable depth octree model with color coded levels (5-Red, 4-Yellow, 3-Cyan)

Fig. 2 Asteroid Itokawa point cloud data with constructed octree

C. Selection of enclosed nodes

Both modeling methods above provide only the list of outer leaf nodes because the point cloud used to build the models contain only the location of surface vertices. In the octree-based mascon approach, the gravitational potential is computed as the summation of potential induced by individual mass concentration. It is essential to identify all the inner leaf nodes that contribute to the volume of an octree model. This section provides a *Section and Boundary* approach to identify the inner leaf nodes in the model, provided the list of occupied outer nodes in the model. Though there are other existing methods to identify whether a point (i.e. octree node's centroid) is inside a polyhedron, this approach is found to be more efficient when dealing with octrees.

This approach starts with the selection of any one coordinate axis that will act a reference axis to group the nodes. After selecting the reference axis (for e.g. x-axis) the boundary coordinates of all the leaf nodes in the octree model are collected. From the list of boundary coordinates, the unique values are then filtered. When the unique values are arranged in order, the range of values extends from minimum to maximum boundary coordinates of the root node along the chosen reference axis. A plane normal to the reference axis is generated at each unique value. The leaf nodes that share their boundaries (either maximum or minimum) with the generated plane are identified and grouped together to form a layer (with grouped nodes) corresponding to each unique value. when the grouped nodes are arranged in 3D, they provide a sliced version of the octree model at the unique reference-axis value. There will be *n-1* layers (with grouped nodes) for n unique values. The node centers of the grouped nodes are projected to the corresponding plane within the layer. The placement of node centers depends upon the octree model. In the uniform-depth octree model, the distance between the leaf node centers is the same because of the constant node sizes across the model. Whereas, in the variable-depth octree model, the distance between the node centers varies depend on their node sizes. Once the node centers are projected onto the plane at each layer, the center coordinates of the occupied outer nodes are used to construct the 2D polygon boundary.

The node center of the remaining nodes in the layer is then validated whether it is located inside or outside the polygon boundary. The nodes that are inside the 2D polygon are marked as occupied. Using the occupied nodes, the second boundary is constructed and the new nodes that form the boundary vertices are marked as outer nodes. The process is repeated at each sectioning layer to identify the list of enclosed nodes using the outer leaf nodes position. The last step adds new outer leaf nodes that are not classified initially due to the sparsity of the point cloud in some regions compared to the element size of the octree nodes. The boundary on each layer is constructed using robust algorithms such as the α-Shape [20] to create a non-convex region boundary that envelops the points. MATLAB's inbuilt alphashape function is primarily used in the simulation setup. The boundary layer selection, in turn, affects the number of bins included in the octree model, proper fit of a boundary layer will ensure proper octree nodes are selected for further computation process. The α-Shape are robust for disjoint enclosures arising from holes or deep craters in the models. One of the limitations of the octree model is that the holes or craters (on the surface) smaller than the node size

are completely enclosed within the node and it is difficult to model them without high resolution octree model.

The entire process is repeated at each unique boundary value along the selected axis to identify all leaf nodes that contribute to the volume of the octree model. After the final list of nodes is collected, the entire volume of the octree model is computed by summing the volume of the individual nodes and with the known density, the mass of the object is calculated. A sample layer from an octree model of asteroid Itokawa is shown in fig. 3, with the individual bin's centroid represented as "○" , the occupied (i.e. surface) bins as "⊗" and the enclosed bins as "●".

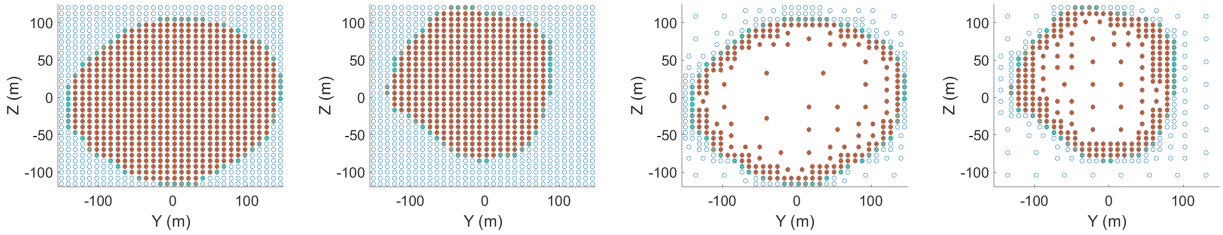

(a) Uniform octree-layer 9 (b) Uniform octree-layer 21 (c) Variable octree-layer 9 (d) Variable octree-layer 21

Fig. 3 Sample layers from asteroid Itokawa octree model (with occupied, empty and enclosed nodes)

III. Gravitational Potential

The total number of octree nodes N is equal to the sum of outer nodes N_{out} and inner nodes N_{in} in the octree model. Each octree node is assumed to have a uniform density and its mass is concentrated on the centroid x_c^i. The mass (m_i) of an i^{th} octree node is determined from the node's density and volume ($m_i = \rho_i.V_i$).

The constructed octree model has a larger volume compared to the polyhedron volume and thus with the same density values, the octree model possess additional mass than the polyhedron model. This extra volume is contributed by the outer octree nodes (which are sparsely occupied), and hence to equalize the octree's mass to the polyhedron's mass. To remove the additional mass contributed by the outer nodes, the density of the outer nodes are modified so that the total mass remains the same. The new density of the outer nodes is given by ρ_{outer}, is provided below.

$$\rho_{outer} = \left(1 - \frac{Vol_{diff}}{Vol_{outer}}\right) * \rho_{asteroid} \tag{1}$$

where $Vol_{diff} = \sum_{i=1}^{N} V_i - V_{poly}$, N denotes number of octree nodes, V_i denotes volume of the individual nodes, V_{poly} is the volume of the polyhedron model. While applying the density values to the octree nodes to compute the center of mass, there will be a small difference (in few centimeters) between the computed and true value. This displacement can be removed by fitting the density value of the nodes so that the center of mass of the octree model matches the true value. However, the associated computation cost will be higher depending on the number of nodes. Hence in this work the calculated density values from eq. (1) are directly substituted in the further calculations.

The gravitational potential (**U**) at any point k is calculated as the sum of potential generated by an individual octree nodes or mass elements m_i and defined as below.

$$\mathbf{U} = \sum_{i=1}^{N} \frac{\mu_i}{r_i} = \sum_{i=1}^{N} \frac{G\,\rho_i V_i}{r_i} \tag{2}$$

where $r_i = \sqrt{\epsilon^2 + \zeta^2 + \eta^2}$ the distance from the i^{th} node's centroid C_i (x_c^i, y_c^i, z_c^i) to the external point k (x_k, y_k, z_k); $\epsilon = x_k - x_c^i$, $\zeta = y_k - y_c^i$, $\eta = z_k - z_c^i$. Gravitational parameter μ_i (μ_{g_i}) is defined as $\mu_i = G.m_i$ where G is the gravitational constant.

When computing the gravitational potential of the points on the asteroid's surface, the field point's location will be inside an octree node. Hence, during the potential calculation, the outer nodes are assumed as mascons of a homogeneous sphere of radius R. The value of R is equal to the half the length of the corresponding octree node. When the field point is inside an j^{th} octree node (either identified during octree construction or by verifying $r_i \leq R$), eq. (3) and eq. (5) will include the second term listed in the equations. The gravitational potential **U** is defined as below.

when the point is located outside the octree model

$$\mathbf{U} = \sum_{i=1}^{N} \frac{G\,m_i}{r_i} \tag{3}$$

when the point is located within one of the octree bin

$$\mathbf{U} = \sum_{i=1, i\neq j}^{N} \frac{G\,m_i}{r_i} + \frac{G\,m_j}{2R}\left(3 - \left(\frac{r_j}{R}\right)^2\right) \tag{4}$$

The gravity acceleration $\nabla\mathbf{U}$ is defined as below.

when the point is located outside the octree model

$$\nabla\mathbf{U} = -\sum_{i=1}^{N} \frac{\mu_i}{{r_i}^3} \begin{pmatrix} \epsilon_i \\ \zeta_i \\ \eta_i \end{pmatrix} \tag{5}$$

when the point is located within one of the octree bin

$$\nabla\mathbf{U} = -\sum_{i=1, i\neq j}^{N} \left(\frac{\mu_i}{{r_i}^3} \begin{pmatrix} \epsilon_i \\ \zeta_i \\ \eta_i \end{pmatrix} + \frac{\mu_j}{R^3} \begin{pmatrix} \epsilon_j \\ \zeta_j \\ \eta_j \end{pmatrix} \right) \tag{6}$$

The Hessian of the potential $\nabla\nabla\mathbf{U}$ is calculated as shown in eq. (8).

$$\nabla\nabla\mathbf{U} = \begin{bmatrix} U_{\epsilon\epsilon} & U_{\epsilon\zeta} & U_{\epsilon\eta} \\ U_{\zeta\epsilon} & U_{\zeta\zeta} & U_{\zeta\eta} \\ U_{\eta\epsilon} & U_{\eta\zeta} & U_{\eta\eta} \end{bmatrix} \tag{7}$$

when the point is located outside the octree model

$$
\begin{aligned}
U_{\epsilon\epsilon} &= \sum_{i=1}^{N} \frac{\partial^2 U}{\partial \epsilon_i^2} = \sum_{i=1}^{N} \left(\frac{\partial}{\partial \epsilon_i}\right)\left(\frac{\partial U}{\partial \epsilon_i}\right) = \sum_{i=1}^{N} \frac{3\mu_i \epsilon_i^2}{{r_i}^5} - \sum_{i=1}^{N} \frac{\mu_i}{{r_i}^3} \\
U_{\zeta\zeta} &= \sum_{i=1}^{N} \frac{3\mu_i \zeta_i^2}{{r_i}^5} - \sum_{i=1}^{N} \frac{\mu_i}{{r_i}^3};\ \ U_{\eta\eta} = \sum_{i=1}^{N} \frac{3\mu_i \eta_i^2}{{r_i}^5} - \sum_{i=1}^{N} \frac{\mu_i}{{r_i}^3} \\
U_{\epsilon\zeta} &= \sum_{i=1}^{N} \frac{3\mu_i \epsilon_i \zeta_i}{{r_i}^5};\ U_{\epsilon\zeta} = U_{\zeta\epsilon} \\
U_{\epsilon\eta} &= \sum_{i=1}^{N} \frac{3\mu_i \epsilon_i \eta_i}{{r_i}^5};\ U_{\epsilon\eta} = U_{\eta\epsilon} \\
U_{\zeta\eta} &= \sum_{i=1}^{N} \frac{3\mu_i \zeta_i \eta_i}{{r_i}^5};\ U_{\zeta\eta} = U_{\eta\zeta}
\end{aligned}
\tag{8}
$$

when the point is located within one of the octree bin

$$
\begin{aligned}
U_{\epsilon\epsilon} &= \sum_{i=1, i\neq j}^{N} \left(\frac{3\mu_i \epsilon_i^2}{{r_i}^5} + \frac{3\mu_j \epsilon_j^2}{R^5}\right) - \sum_{i=1, i\neq j}^{N} \left(\frac{\mu_i}{{r_i}^3} + \frac{\mu_j}{R^3}\right) \\
U_{\zeta\zeta} &= \sum_{i=1, i\neq j}^{N} \left(\frac{3\mu_i \zeta_i^2}{{r_i}^5} + \frac{3\mu_j \zeta_j^2}{R^5}\right) - \sum_{i=1, i\neq j}^{N} \left(\frac{\mu_i}{{r_i}^3} + \frac{\mu_j}{R^3}\right) \\
U_{\eta\eta} &= \sum_{i=1, i\neq j}^{N} \left(\frac{3\mu_i \eta_i^2}{{r_i}^5} + \frac{3\mu_j \eta_j^2}{R^5}\right) - \sum_{i=1, i\neq j}^{N} \left(\frac{\mu_i}{{r_i}^3} + \frac{\mu_j}{R^3}\right) \\
U_{\epsilon\zeta} &= \sum_{i=1, i\neq j}^{N} \left(\frac{3\mu_i \epsilon_i \zeta_i}{{r_i}^5} + \frac{3\mu_j \epsilon_j \zeta_j}{R^5}\right);\ U_{\epsilon\zeta} = U_{\zeta\epsilon} \\
U_{\epsilon\eta} &= \sum_{i=1, i\neq j}^{N} \left(\frac{3\mu_i \epsilon_i \eta_i}{{r_i}^5} + \frac{3\mu_j \epsilon_j \eta_j}{R^5}\right);\ U_{\epsilon\eta} = U_{\eta\epsilon} \\
U_{\zeta\eta} &= \sum_{i=1, i\neq j}^{N} \left(\frac{3\mu_i \zeta_i \eta_i}{{r_i}^5} + \frac{3\mu_j \zeta_j \eta_j}{R^5}\right);\ U_{\zeta\eta} = U_{\eta\zeta}
\end{aligned}
\tag{9}
$$

IV. Numerical Simulations

The point cloud data of asteroid Itokawa and asteroid Toutatis, available in [21] are used in the simulations presented in this section. The surface mesh generated using the vertices and faces data for both asteroids are shown in fig.4. The two chosen asteroids are of different size range; Itokawa measures about $560 \times 305 \times 242$ meters whereas Toutatis is bigger than Itokawa and measures $2.28 \times 1.90 \times 4.58$ km. The models are simulated in MATLAB and the CPU configuration including an Intel Core i7-6700 with a processing speed of 3.4 GHz is used. Both variable-depth and uniform-depth octree approaches are simulated for the two cases presented below. The estimated results of the gravitational potential and the gravity acceleration from the two octree approaches are compared against the classic polyhedron method.

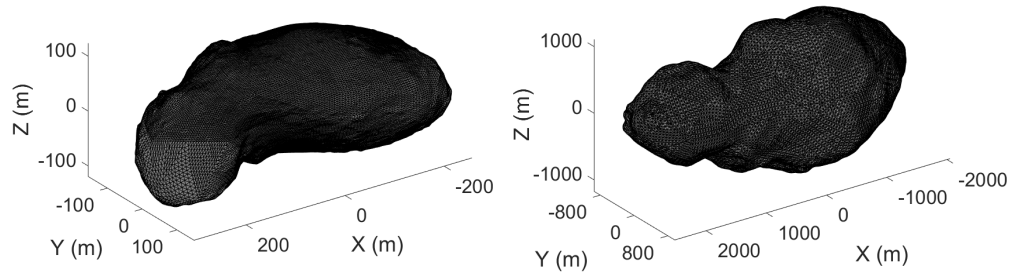

(a) asteroid Itokawa (b) asteroid Toutatis

Fig. 4 Polyhedron model

A. Simulation Cases

1. Case-I : Asteroid surface

The gravitational potential and the acceleration calculated on the asteroid's surface using the location of vertices. The shape model of the asteroid Itokawa has 25,350 vertices (points) whereas the asteroid Toutatis has 20,000 vertices (points). The octree models created using the points as a base reference will be used in the simulation.

2. Case-II : Region around Asteroid

In this case, the gravitational potential and acceleration are calculated for the region around asteroids. A uniformly distributed grid points are generated in XY plane around the asteroid and the boundary limits to generate the points are set to 1.25 times the maximum asteroid dimensions. The number of points generated in the region around Itokawa are 8268 points and for Toutatis are 8803 points.

B. Methods

1. Uniform depth octree

In the uniform-depth approach, the nodes are divided recursively until all the leaf nodes are in the same octree level. To efficiently create an uniform-depth octree model, at first the variable-depth octree model of equal tree depth is constructed and the occupied nodes are identified. Later, the occupied nodes divided to final octree depth according to the uniform-depth octree requirements, i.e., all the octree nodes are divided at each level and the total number of nodes increases by eight times (8x) at each level. This approach is highly efficient and saves significant time in model construction by avoiding division of the non-occupied octree nodes. The leaf nodes are validated for points occupancy and the octree model is created. For simulation purposes, two uniform-depth octree models are created for each asteroid. The octree depth of these models are set to level-7 and level-8 and their final leaf node dimensions corresponds to $(\frac{1}{128})$ and $(\frac{1}{256})$ of octree root node dimensions. The above octree models are represented as $\mathbf{Uni_{128}}$ and $\mathbf{Uni_{256}}$ respectively.

The dimensions of the node elements for the two octree models are summarized in table 1. The summary of total nodes and the number of occupied nodes for each asteroid model is provided in table 2.

2. Variable depth octree

As mentioned in section II.B.2, during the construction of the variable-depth octree model, the nodes are validated for point occupancy before being divided. The nodes are divided only if a node is occupied and bigger than the allowed size limits. Like the previous case, two variable-depth octree models are created for each asteroid and the minimum node dimension limits are $(\frac{1}{128})$ and $(\frac{1}{256})$ of asteroid dimensions, the models will be represented as $\mathbf{Var_{128}}$ and $\mathbf{Var_{256}}$ respectively. Even though in this method, the octree is of the same depth as the uniform-depth octree, the number of node elements is significantly less and this provides computation advantage. For example, the total occupied nodes in the $\mathbf{Var_{256}}$ model are nearly half the occupied nodes in $\mathbf{Uni_{128}}$ model. The total number of octree nodes and the number of occupied nodes for each asteroid model is provided in table 2. The occupied nodes in $\mathbf{Var_{256}}$ model can be found in different octree levels varying from level-3 to level-8.

Table 1 Details of the density and size of the asteroid models in simulation

Asteroid	Density (kg/m^3)	Asteroid size (m)	Cube length $(\frac{1}{128})$ (m)	Cube length $(\frac{1}{256})$ (m)
Itokawa	1.85×10^3	$561.6 \times 305.1 \times 243.4$	4.8	2.4
Toutatis	2.10×10^3	$2281.7 \times 1914.3 \times 4581.0$	39.5	19.75

3. Polyhedron approach

In this approach, a constant density polyhedron is assumed and a polyhedral mesh is constructed with vertices (V), faces (F) and edges (E). The details of the number of vertices (points), edges and faces for each asteroid model is summarized in table 2. To construct the polyhedron mesh, the point cloud data is used as vertices and in addition, the face data of connected vertices are included. The 3D-mesh of asteroid Itokawa has 49,152 faces and 73,728 edges with mean edge size of 4.7 m and max of 17.0 m and Toutatis has 39996 faces and 59,994 edges with mean edge size of 37.9 m and max of 73.8 m. The gravitational potential U, acceleration ∇U and Hessian $\nabla\nabla U$ of a constant density polyhedron as described in [11] are provided below.

$$U = \frac{1}{2}G\rho \sum_{e \in edges} \mathbf{r}_e.\mathbf{E}_e.\mathbf{r}_e.L_e - \frac{1}{2}G\rho \sum_{f \in faces} \mathbf{r}_f.\mathbf{F}_f.\mathbf{r}_f.\omega_f \tag{10}$$

$$\nabla U = -G\rho \sum_{e \in edges} \mathbf{E}_e.\mathbf{r}_e.L_e + G\rho \sum_{f \in faces} \mathbf{F}_f.\mathbf{r}_f.\omega_f \tag{11}$$

$$\nabla\nabla U = G\rho \sum_{e \in edges} \mathbf{E}_e . L_e + G\rho \sum_{f \in faces} \mathbf{F}_f . \omega_f \tag{12}$$

Table 2 Details of octree and polyhedron models used in numerical simulation

		$\mathbf{Var_{128}}$	$\mathbf{Var_{256}}$	$\mathbf{Uni_{128}}$	$\mathbf{Uni_{256}}$	Polyhedron
Itokawa	occupied nodes	32,820	93,294	170,909	1,311,078	73,728 (edges)
(25,350 points)	total nodes	58,865	190,657	216,681	1,583,953	49,152 (faces)
Toutatis	occupied nodes	27,376	78,189	131,550	1,005,023	59,994 (edges)
(20,000 points)	total nodes	49,105	160,417	168,161	1,220,561	39,996 (faces)

V. Results

A. Case-I: Asteroid surface

The gravitational potential and acceleration calculated on the surface of two asteroids (Itokawa and Toutatis) using the octree and polyhedron models are shown in figs. 5–8. The sub-figure (*d, e*) in figs. 5–8 shows the relative error of gravitational potential and acceleration for different octree models with respect to the polyhedron model (which is assumed to be highly accurate). The sub-figure (*f*) in figs. 5–8 shows the computed mean relative error for different octree methods. The computation time for each model is summarized in table 3. The potential and acceleration values, as well as the error and deviation for each octree model compared to the polyhedron model for both asteroids, is summarized in table 4 and table 5.

Table 3 Summary of computation time

		$\mathbf{Var_{128}}$	$\mathbf{Var_{256}}$	$\mathbf{Uni_{128}}$	$\mathbf{Uni_{256}}$	Polyhedron
Case -I	Itokawa	34 s	1 m 49 s	3 m 30 s	27 m 7 s	9 m 50 s
	Toutatis	22 s	1 m 12 s	2 m 08 s	16 m 20 s	5 m 13 s
Case -II	Itokawa	11 s	35 s	1 m 08 s	8 m 39 s	3 m 05 s
	Toutatis	10 s	31 s	56 s	7 m 9 s	2 m 17 s

The mean relative error of the potential calculated using both octree models varies between $0.1 \sim 0.01\%$ ($10^{-3} \sim 10^{-4}$). The variable-depth method closely follows the uniform-depth octree method and the mean relative error of potential on the asteroid Toutatis's surface is similar to the asteroid Itokawa's surface. The uniform octree model $\mathbf{Uni_{256}}$ provides higher accuracy compared to all other octree models but it is computationally expensive as it has a larger number of mascon elements ($\sim$ 1million elements). The results of variable-depth model $\mathbf{Var_{128}}$ and uniform-depth model $\mathbf{Uni_{128}}$ are nearly the same. The advantage of the variable-depth model is that it uses nearly $(\frac{1}{6})^{th}$ number of nodes in uniform model of the same depth and this inturn reduces the computation time. When dividing the octree model

to next level, the $\mathbf{Uni_{256}}$ model provide better accuracies in potential computation however the $\mathbf{Var_{256}}$ model matches the acceleration accuracies of $\mathbf{Uni_{256}}$ model and with significantly less computation time. The results of potential and acceleration near the surface of the target body highlights the advantages of variable-depth model comparing to uniform-depth model. The $\mathbf{Var_{256}}$ model even has less number of node elements than the $\mathbf{Uni_{128}}$ model and offers better performance and saves half the computation time. The computation time of the three octree models $\mathbf{Var_{128}}$, $\mathbf{Var_{256}}$ and $\mathbf{Uni_{128}}$ are significantly less than the time taken during the polyhedron method. However, the computation time of $\mathbf{Uni_{256}}$ model is 3× more than the polyhedron method and this due to a large number of occupied nodes (nearly >10x than $\mathbf{Var_{256}}$ model).

Table 4 Comparison of results (Case -I) on asteroid Itokawa surface

		$\mathbf{Var_{128}}$	$\mathbf{Var_{256}}$	$\mathbf{Uni_{128}}$	$\mathbf{Uni_{256}}$	Polyhedron
potential	min	−0.0148	−0.0148	−0.0148	−0.0148	−0.0148
($J\ kg^{-1}$)	max	−0.0092	−0.0092	−0.0092	−0.0092	−0.0093
error ($J\ kg^{-1}$)	μ	2.12×10^{-6}	-1.47×10^{-6}	1.66×10^{-6}	5.98×10^{-7}	
	σ	6.29×10^{-6}	5.75×10^{-6}	4.82×10^{-6}	1.80×10^{-6}	
	$\xi_{<5}$ | $\xi_{<1}$	100 | 100	100 | 100	100 | 100	100 | 100	
acceleration (norm)	min	5.59×10^{-5}	5.65×10^{-5}	5.59×10^{-5}	5.69×10^{-5}	5.73×10^{-5}
($m\ s^{-2}$)	max	7.98×10^{-5}	8.11×10^{-5}	7.89×10^{-5}	8.05×10^{-5}	8.02×10^{-5}
error ($m\ s^{-2}$)	μ	2.02×10^{-6}	9.20×10^{-7}	1.98×10^{-6}	8.85×10^{-7}	
	σ	5.19×10^{-7}	4.19×10^{-7}	3.75×10^{-7}	2.28×10^{-7}	
	$\xi_{<5}$ | $\xi_{<1}$	99.45 | 0.25	99.95 | 36.46	99.0 | 0.5	100 | 35.75	

$\xi_{<5}$ - percentage of values < 5 % error $\xi_{<1}$ - percentage of values < 1 % error

Table 5 Comparison of results (Case -I) on asteroid Toutatis surface

		$\mathbf{Var_{128}}$	$\mathbf{Var_{256}}$	$\mathbf{Uni_{128}}$	$\mathbf{Uni_{256}}$	Polyhedron
potential	min	−0.9840	−0.9843	−0.9841	−0.9843	−0.9844
($J\ kg^{-1}$)	max	−0.5484	−0.5484	−0.5484	−0.5484	−0.5484
error ($J\ kg^{-1}$)	μ	2.1×10^{-4}	4.88×10^{-4}	2.13×10^{-4}	3.56×10^{-5}	
	σ	2.9×10^{-4}	2.2×10^{-4}	2.39×10^{-4}	7.51×10^{-5}	
	$\xi_{<5}$ | $\xi_{<1}$	100 | 100	100 | 100	100 | 100	100 | 100	
acceleration (norm)	min	4.28×10^{-4}	4.37×10^{-4}	4.28×10^{-4}	4.39×10^{-4}	4.44×10^{-4}
($m\ s^{-2}$)	max	6.94×10^{-4}	7.02×10^{-4}	6.87×10^{-4}	7.02×10^{-4}	6.98×10^{-4}
error ($m\ s^{-2}$)	μ	1.84×10^{-5}	7.83×10^{-6}	1.83×10^{-5}	6.53×10^{-6}	
	σ	3.91×10^{-6}	2.91×10^{-6}	3.30×10^{-6}	1.10×10^{-6}	
	$\xi_{<5}$ | $\xi_{<1}$	99.35 | 0.11	100 | 32.24	99.73 | 0	100 | 28.6	

$\xi_{<5}$ - percentage of values < 5 % error $\xi_{<1}$ - percentage of values < 1 % error

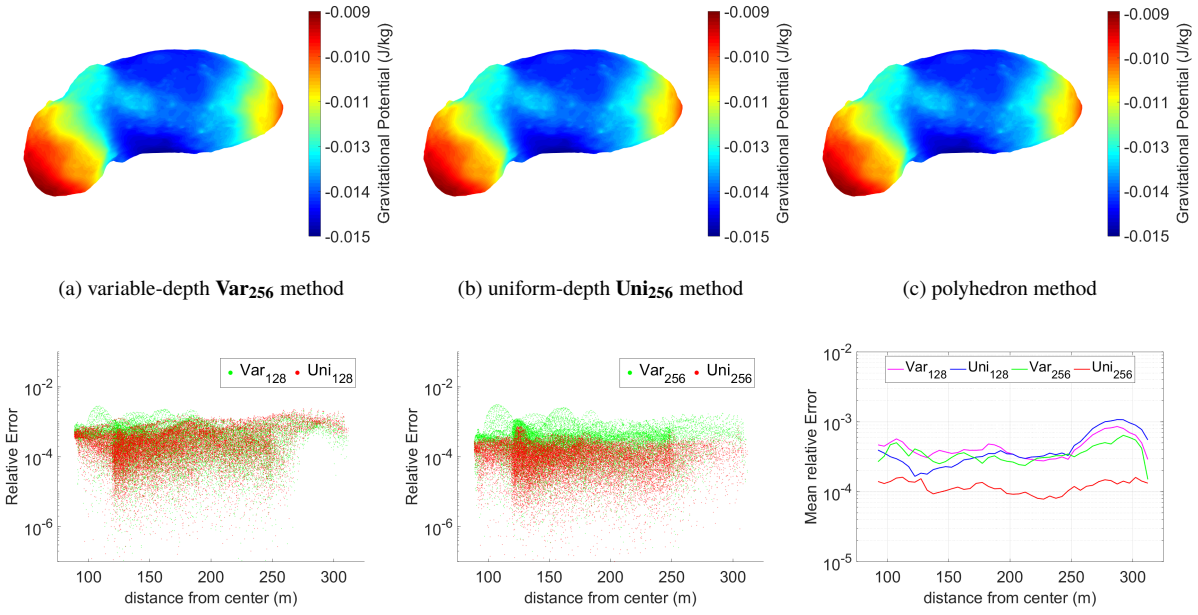

(a) variable-depth $\mathbf{Var_{256}}$ method (b) uniform-depth $\mathbf{Uni_{256}}$ method (c) polyhedron method

(d) relative error ($\frac{1}{128}$) method (e) relative error ($\frac{1}{256}$) method (f) mean relative error

Fig. 5 Gravitational potential on the surface of asteroid Itokawa

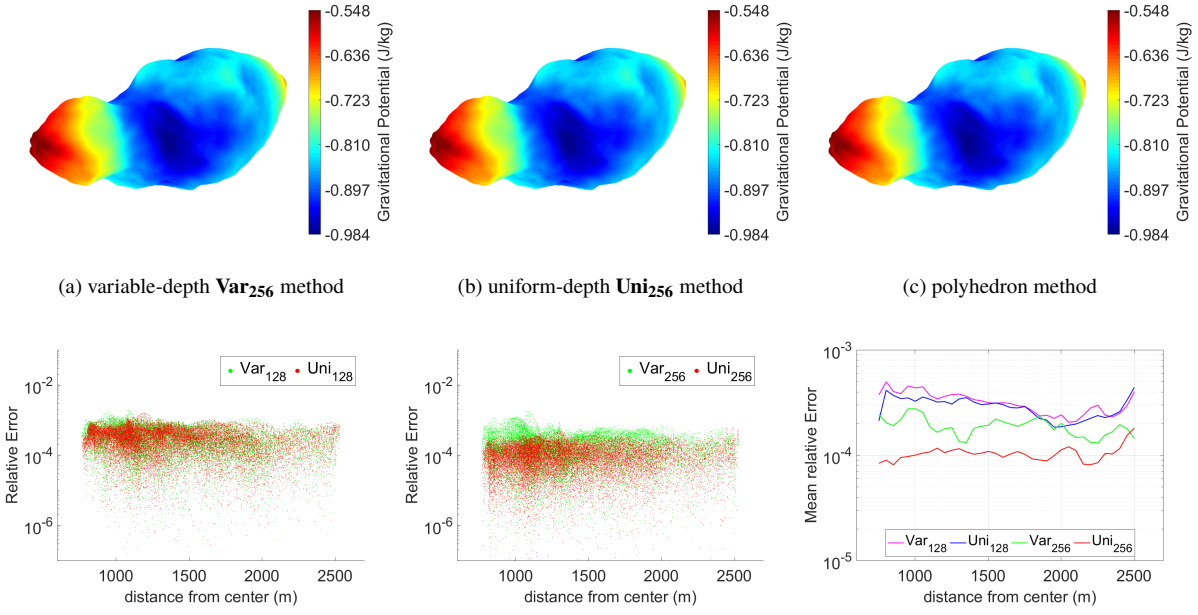

(a) variable-depth $\mathbf{Var_{256}}$ method (b) uniform-depth $\mathbf{Uni_{256}}$ method (c) polyhedron method

(d) relative error ($\frac{1}{128}$) method (e) relative error ($\frac{1}{256}$) method (f) mean relative error

Fig. 6 Gravitational potential on the surface of asteroid Toutatis

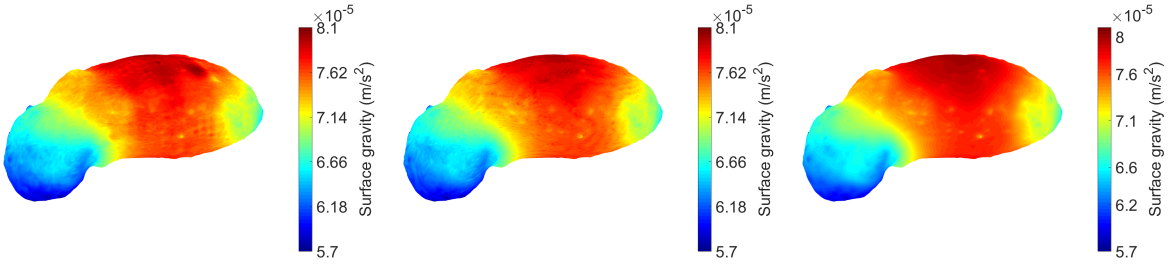

(a) variable-depth $\mathbf{Var_{256}}$ method (b) uniform-depth $\mathbf{Uni_{256}}$ method (c) polyhedron method

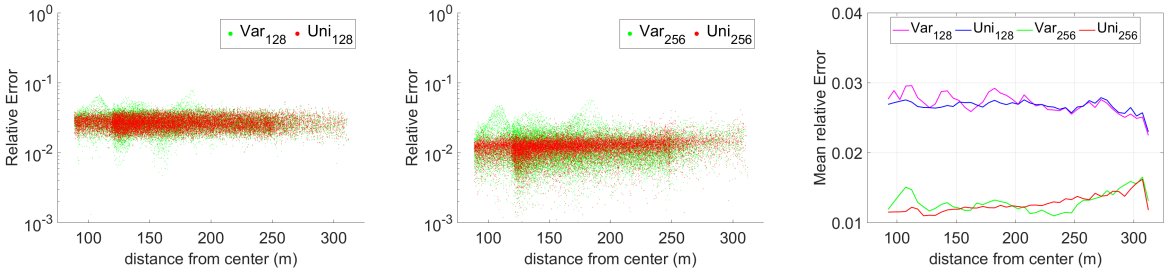

(d) relative error ($\frac{1}{128}$) method (e) relative error ($\frac{1}{256}$) method (f) mean relative error

Fig. 7 Gravitational acceleration (norm) on the surface of asteroid Itokawa

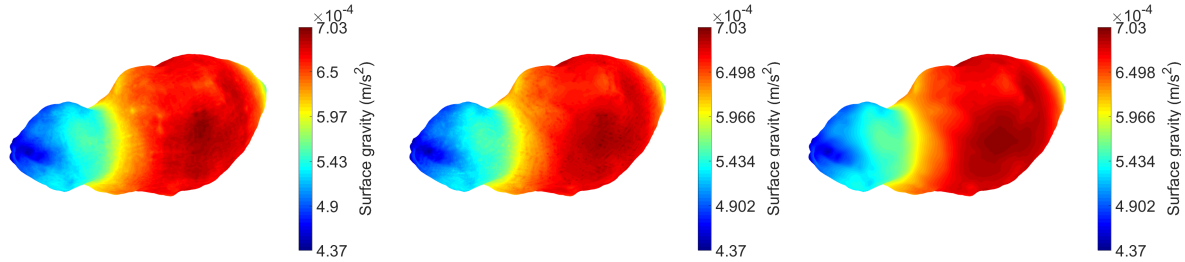

(a) variable-depth $\mathbf{Var_{256}}$ method (b) uniform-depth $\mathbf{Uni_{256}}$ method (c) polyhedron method

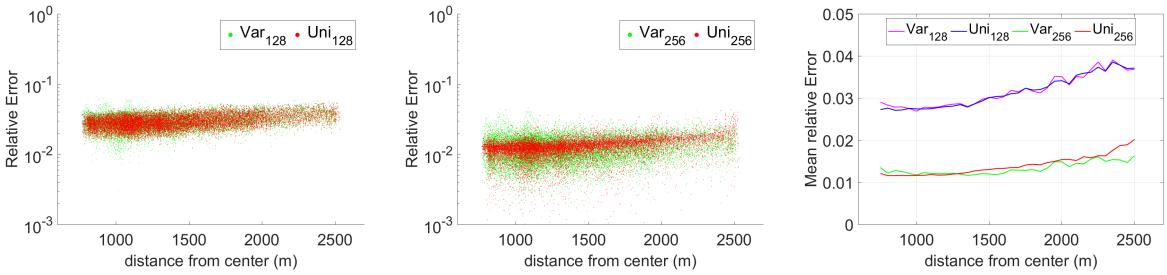

(d) relative error ($\frac{1}{128}$) method (e) relative error ($\frac{1}{256}$) method (f) mean relative error

Fig. 8 Gravitational acceleration (norm) on the surface of asteroid Toutatis

B. Case-II : Region around asteroid

In case-II, the gravity fields are calculated for the region around the asteroid using the octree models and their performances are compared with the polyhedron method. $\mathbf{Var_{128}}$ model performs better at the larger distances compared to $\mathbf{Uni_{128}}$, but in the regions close to surface the uniform-depth model performs better in both asteroids. The performance of $\mathbf{Var_{256}}$ has slightly improved than the $\mathbf{Var_{128}}$ model for both potential and acceleration in the region around the asteroid. In the uniform-depth methods, $\mathbf{Uni_{256}}$ model provide better results than the other octree models. The gravity acceleration in the region around the asteroid Itokawa and Toutatis are shown in fig. 9. The mean relative error of gravitational potential and acceleration compared to the polyhedron method for both asteroids are plotted in fig. 10.

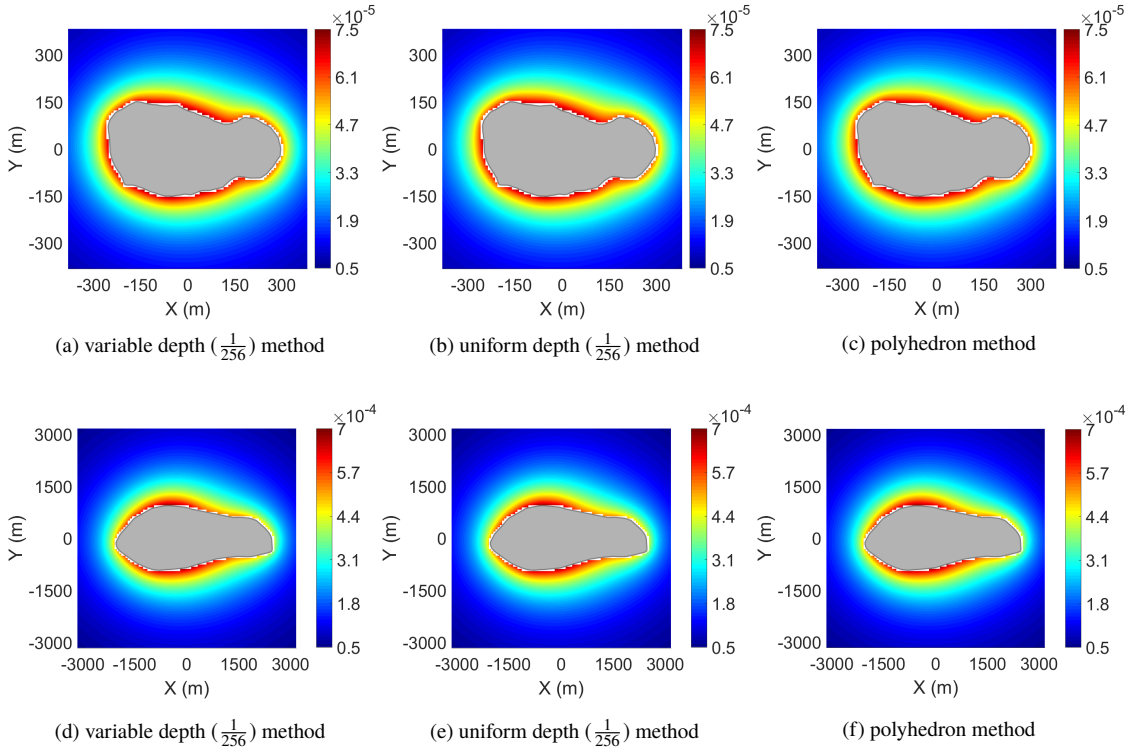

(a) variable depth ($\frac{1}{256}$) method (b) uniform depth ($\frac{1}{256}$) method (c) polyhedron method

(d) variable depth ($\frac{1}{256}$) method (e) uniform depth ($\frac{1}{256}$) method (f) polyhedron method

Fig. 9 Gravitational acceleration (norm) $(in\ m/s^2)$ **near asteroid Itokawa (a-c) and Toutatis (d-f)**

The potential and acceleration errors for both octree approaches compared to the polyhedron method are summarized in table 6. The computational time is similar to the previous case, the time taken for both variable-depth models $\mathbf{Var_{128}}$ and $\mathbf{Var_{256}}$ and uniform-depth $\mathbf{Uni_{128}}$ model is less than the polyhedron model. But the computation time taken for the $\mathbf{Uni_{256}}$ is $2\times \sim 3\times$ more than the time taken for the polyhedron method. Mean relative error of the potential and acceleration computed using the octree models are better in the region around the asteroid (well below 1% at larger distances) when compared to case-I results (on the surface of the asteroid). From the results, it is evident that the variable-depth models offers accuracies similar to the uniform-depth models and also computationally efficient.

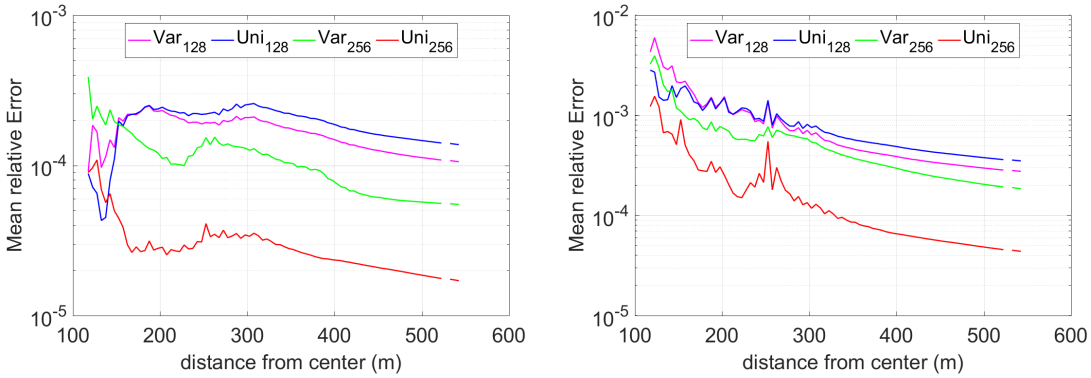

(a) grav. potential error - Itokawa

(b) grav. acceleration error - Itokawa

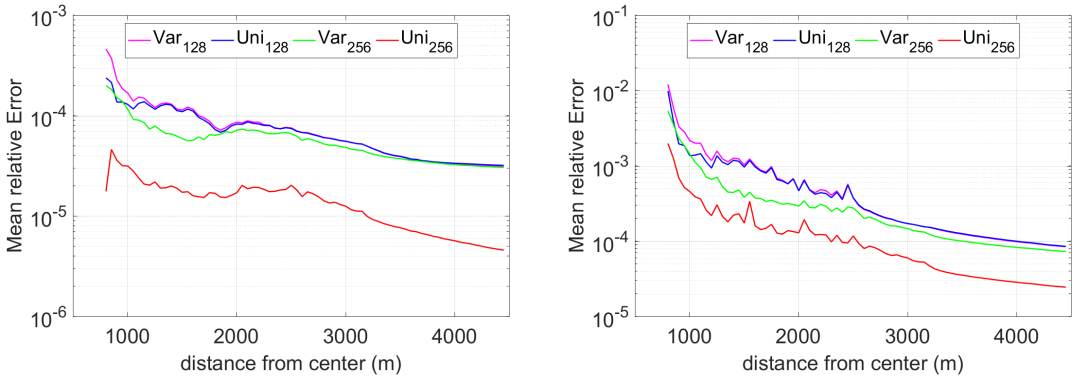

(c) grav. potential error - Toutatis

(d) grav. acceleration error - Toutatis

Fig. 10 Relative error of Potential and acceleration near asteroid Itokawa and Toutatis

C. Discussions

This section discuss the results of octree approach and compares the achieved accuracies with the other mascon models discussed in the earlier research works [11, 14, 16].

Werner and Scheeres [11] have demonstrated that the errors depend on the size of the node elements and shown the impact of the number of mascons 'N' in the uniform mascon model with the accuracy of the model goes as $\frac{1}{N^{\frac{1}{3}}}$. Though the variable-depth octree models have mass elements of different sizes, the achieved accuracies of the model behave as described above. The accuracy of the $\mathbf{Var_{256}}$ model improved by a factor of 10 compared to a lower resolution model $\mathbf{Uni_{128}}$ where the number of mascons is 1000 times lower.

Tardivel [14] highlighted that for small bodies, similar to the size of Itokawa, achieving the low altitude accuracy of 1% threshold requires a minimum of about 100,000 mascons and up to a few tens of millions for 0.1 % accuracy threshold. The variable-depth octree model achieves similar accuracy threshold, where $\mathbf{Var_{256}}$ model with approximately 100,000 mascons achieved nearly $1\%(10^{-2})$ relative error on the asteroid's surface. However, the statement also holds true in the case of larger asteroid Toutatis where the variable-depth model $\mathbf{Var_{256}}$ behaves in a similar fashion. In

Table 6 Comparison of results (Case-II) for region near an asteroid

			$\mathbf{Var_{128}}$	$\mathbf{Var_{256}}$	$\mathbf{Uni_{128}}$	$\mathbf{Uni_{256}}$
Itokawa	potential error	μ	-3.64×10^{-6}	2.57×10^{-7}	-3.35×10^{-7}	-2.50×10^{-9}
(8268 points)	($J\ kg^{-1}$)	σ	1.80×10^{-6}	1.12×10^{-6}	2.10×10^{-6}	3.10×10^{-7}
		$\xi_{<5}$ | $\xi_{<1}$	100 | 100	100 | 100	100 | 100	100 | 100
	acceleration error	μ	2.43×10^{-8}	1.6×10^{-8}	2.49×10^{-8}	5.70×10^{-9}
	($m\ s^{-2}$)	σ	6.14×10^{-8}	2.88×10^{-8}	5.79×10^{-8}	2.35×10^{-8}
		$\xi_{<5}$ | $\xi_{<1}$	100 | 99.85	100 | 100	100 | 99.57	100 | 100
Toutatis	potential error	μ	-1.77×10^{-5}	-1.76×10^{-5}	-1.61×10^{-5}	-2.61×10^{-6}
(8803 points)	($J\ kg^{-1}$)	σ	5.73×10^{-5}	4.25×10^{-5}	5.33×10^{-5}	1.18×10^{-5}
		$\xi_{<5}$ | $\xi_{<1}$	100 | 100	100 | 100	100 | 100	100 | 100
	acceleration error	μ	1.65×10^{-7}	8.44×10^{-8}	1.47×10^{-7}	3.28×10^{-8}
	($m\ s^{-2}$)	σ	6.85×10^{-7}	2.73×10^{-7}	6.24×10^{-7}	1.19×10^{-7}
		$\xi_{<5}$ | $\xi_{<1}$	100 | 99.62	100 | 99.99	100 | 99.66	100 | 99.99

$\xi_{<5}$ - percentage of values < 5 % error $\xi_{<1}$ - percentage of values < 1 % error

the region around asteroid (especially at lower altitudes), the accuracies are well below the $1\%(10^{-2})$ threshold limit for the two simulated variable-depth octree models. The unequal packaging in Tardival's work is comparable to the variable-depth octree model because both models enclose the mascons of different sizes. The unequal packaging creates larger pockets of masses within the model with higher bulk densities and this creates gaps between the larger mascons. Later, the gaps are filled with smaller mascons having lower density values. This density variation significantly impacts the computation of the gravitational potential and its derivatives. The unequal packaging has lower porosity levels compared to the variable-depth models and the changes to the bulk density values of the mascon elements have a greater influence in the computation of the gravitational field at higher altitudes, where the errors are significantly higher. This highlights the impact of the density values on the computed potential and acceleration values. The relative error on gravitational acceleration measured in Tardival's work was around 1% for different packing arrangements for a mascon radius of 5 m at an altitude of 1 m above Itokawa's surface. The relative potential error on the surface might be a little higher, however, it is comparable to the results of variable-depth octree model $\mathbf{Var_{256}}$ on the surface of asteroid Itokawa.

In another research work, Wittick and Russell [16] investigated different mascon models with an intent to minimize the number of elements and to optimize the placement of elements to improve the accuracy levels. Wittick's core-shell approach is comparable to the variable-depth approach presented in this work. In the core-shell approach, using a series of scaled-down shape models they defined the cores of the surrounding shells. They used large mascons deep within the body, sometimes with their own limited spherical harmonics, and small mascons close to the surface. Wittick's work represented the error averaged over the altitudes and hence it is difficult to compare the performance with the octree models. The results suggest that the core-shell approach accuracies are better compared to uniform and multi-layer uniform methods. In certain simulated cases, core-shell approach achieved a significant gain in accuracy over other models with larger memory allocations.

The octree model constructed in this work does not constrain the range of the octree depths and this allows the occupied inner nodes of any tree-depth. This leads to the condition that the model only guarantees the outer nodes in a desired tree-depth, whereas the inner nodes (possibly bigger) may appear close to the surface within the model. This might affect the accuracies of the computed potential values. However, the octree model provides the flexibility to constrain the number of levels in tree depths and this significantly reduces the appearance of much larger nodes close to the surface within the model. This requires a hybrid approach combining both the uniform-depth octree (till the lower level) and the variable-depth octree (lower to a higher level).

Overall, the variable-depth octree models $\mathbf{Var_{128}}$ and $\mathbf{Var_{256}}$ matched the performance of corresponding uniform models near the surface, and also on the regions around the asteroid. As Tardival highlighted, any sound enough mathematical representation with the accuracies close to or within 1% of homogeneous polyhedron may be given full consideration in terms of preliminary mission planning and theoretical astrodynamics.

VI. Conclusions

The intent of this work is to introduce an octree-based mascon representation to compute the gravitational potential and its derivatives of an irregular celestial body. To model an irregular celestial body into octrees, this work presented two octree modeling approaches, namely Variable-depth octree and Uniform-depth octree. The variable-depth model has leaf nodes spread across different tree levels with node sizes varying accordingly. Whereas in the uniform-depth model, the leaf nodes size is constant across the model. In the variable-depth modeling approach, the nodes are divided based on two conditions, the point(s) occupancy and a pre-defined tree-depth of an occupied leaf node. The number of elements in the variable-depth octree is significantly less when compared to the uniform-depth octree because the enclosed empty nodes are left undivided in the former approach. To select the enclosed inner nodes in both the octree model a new approach named *section and boundary* was introduced. The mass of an octree model is matched with the mass of the polyhedron through modifying the density values of the outer octree nodes and resulted in the different density values between the inner and outer nodes.

The simulations are carried out for two test cases: in case one, the gravity potential and acceleration are calculated on the surface of the asteroid and in case two, the potential and acceleration are computed for uniformly distributed points in the region around the asteroid. The simulations are carried out on the models of the asteroids Itokawa and Toutatis for both the octree-mascon and the polyhedron approach and their results are presented in detail. When computing the potential and acceleration, the points on the asteroid's surface are enclosed within octree nodes and hence during computation they are assumed to be inside a homogeneous sphere. The results are shown in table 3 and suggests that the octree approach is more computationally efficient than the polyhedron approach. The time required for the numerical simulation of the three octree models $\mathbf{Var_{128}}$, $\mathbf{Var_{256}}$ and $\mathbf{Uni_{128}}$ are less than the polyhedron model. But the computation time taken for the $\mathbf{Uni_{256}}$ is triple the time taken for the polyhedron method and this is due to the

number of mascon elements within the model. Within the octree approach, the variable-depth octree is computationally efficient than the uniform-depth approach and offers the accuracy similar to that of uniform-depth approach near the surface of an asteroid. Whereas in the regions around an asteroid, the accuracies are equal when the mascon sizes are bigger and as the size reduces, the uniform-depth model provides better accuracy with a higher computation cost. Overall, the results suggest that the octree-based approaches are computationally efficient and offer a good alternative for construction of mascon models to study the gravitational field of a small body. In future work, the octree models will be used within simultaneous localization and mapping framework to solve for the inverse problem of estimating asteroid's mass distribution. Within the framework, the density values of the octree nodes can represent a part of state variables to be estimated and the framework can use filtering/smoothing-based state estimation approach to solve for the optimal state variables.

References

[1] Fujiwara, A., Kawaguchi, J., Yeomans, D. K., Abe, M., Mukai, T., Okada, T., Saito, J., Yano, H., Yoshikawa, M., Scheeres, D. J., Barnouin-Jha, O., Cheng, A. F., Demura, H., Gaskell, R. W., Hirata, N., Ikeda, H., Kominato, T., Miyamoto, H., Nakamura, A. M., Nakamura, R., Sasaki, S., and Uesugi, K., "The Rubble-Pile Asteroid Itokawa as Observed by Hayabusa," *Science*, Vol. 312, No. 5778, 2006, pp. 1330–1334. doi:10.1126/science.1125841.

[2] Evans, L. G., Starr, R. D., Brückner, J., Reedy, R. C., Boynton, W. V., Trombka, J. I., Goldsten, J. O., Masarik, J., Nittler, L. R., and Mccoy, T. J., "Elemental composition from gamma ray spectroscopy of the NEAR Shoemaker landing site on 433 Eros," *Meteoritics & Planetary Science*, Vol. 36, No. 12, 2001, pp. 1639–1660. doi:10.1111/j.1945-5100.2001.tb01854.x.

[3] Glassmeier, K.-H., Boehnhardt, H., Koschny, D., Kührt, E., and Richter, I., "The Rosetta Mission: Flying Towards the Origin of the Solar System," *Space Science Reviews*, Vol. 128, No. 1, 2007, pp. 1–21. doi:10.1007/s11214-006-9140-8.

[4] Tsuda, Y., Yoshikawa, M., Abe, M., Minamino, H., and Nakazawa, S., "System design of the hayabusa 2-asteroid sample return mission to 1999 JU3," *Acta Astronautica*, Vol. 91, 2013, pp. 356–362. doi:10.1016/j.actaastro.2013.06.028, URL `http://dx.doi.org/10.1016/j.actaastro.2013.06.028`.

[5] Beshore, E., Lauretta, D., Boynton, W., Shinohara, C., Sutter, B., Everett, D., Gal-Edd, J., Mink, R., Moreau, M., and Dworkin, J., "The OSIRIS-REx asteroid sample return mission," *IEEE Aerospace Conference Proceedings*, Vol. 2015-June, 2015. doi:10.1109/AERO.2015.7118989.

[6] Cheng, A., Atchison, J., Kantsiper, B., Rivkin, A., Stickle, A., Reed, C., Galvez, A., Carnelli, I., Michel, P., and Ulamec, S., "Asteroid Impact and Deflection Assessment mission," *Acta Astronautica*, Vol. 115, 2015, pp. 262 – 269. doi:https://doi.org/10.1016/j.actaastro.2015.05.021.

[7] Erickson, K. R., "Optimal Architecture for an Asteroid Mining Mission: Equipment Details and Integration," *American Institute of Aeronautics and Astronautics*, , No. September, 2006, pp. 1–17. doi:10.2514/6.2006-7504.

[8] Sonter, M. J., "The technical and economic feasibility of mining the near-earth asteroids," *Acta Astronautica*, Vol. 41, No. 4-10, 1997, pp. 637–647. doi:10.1016/S0094-5765(98)00087-3.

[9] MacMillan, W., *The Theory of the Potential*, Dover books on physics and mathematical physics, Dover Publications, 1958.

[10] Balmino, G., "Gravitational potential harmonics from the shape of an homogeneous body," *Celestial Mechanics and Dynamical Astronomy*, Vol. 60, No. 3, 1994, pp. 331–364. doi:10.1007/BF00691901, URL https://doi.org/10.1007/BF00691901.

[11] Werner, R. A., and Scheeres, D. J., "Exterior Gravitation of a Polyhedron Derived and Compared with Harmonic and Mascon Gravitation Representations of Asteroid 4769 Castalia," *Celestial Mechanics and Dynamical Astronomy*, Vol. 65, No. 3, 1997, pp. 313–344.

[12] Geissler, P., Petit, J. M., Durda, D. D., Greenberg, R., Bottke, W., Nolan, M., and Moore, J., "Erosion and ejecta reaccretion on 243 Ida and its moon," *Icarus*, Vol. 120, No. 1, 1996, pp. 140–157. doi:10.1006/icar.1996.0042.

[13] Chanut, T., Aljbaae, S., and Carruba, V., "Mascon gravitation model using a shaped polyhedral source," *Monthly Notices of the Royal Astronomical Society*, Vol. 450, No. 4, 2015, pp. 3742–3749. doi:10.1093/mnras/stv845.

[14] Tardivel, S., "The Limits of the Mascons Approximation of the Homogeneous Polyhedron," *AIAA/AAS Astrodynamics Specialist Conference*, , No. September, 2016, pp. 1–13. doi:10.2514/6.2016-5261, URL http://arc.aiaa.org/doi/10.2514/6.2016-5261.

[15] Pearl, J. M., and Hitt, D. L., "Asteroid Gravitational Models Using Mascons Derived from Polyhedral Sources," *AIAA/AAS Astrodynamics Specialist Conference*, , No. September, 2016, pp. 1–16. doi:10.2514/6.2016-5260.

[16] Wittick, P. T., and Russell, R. P., "Mascon Models for Small Body Gravity Fields," *AAS/AIAA Astrodynamics Specialist Conference*, Stevenson, WA, 2017.

[17] Meagher, D., "Geometric modeling using octree encoding," *Computer Graphics and Image Processing*, Vol. 19, No. 2, 1982, pp. 129–147. doi:10.1016/0146-664X(82)90104-6.

[18] Chien, C. H., and Aggarwal, J. K., "Volume/surface octrees for the representation of three-dimensional objects," *Computer Vision, Graphics, and Image Processing*, Vol. 36, No. 1, 1986, pp. 100–113. doi:https://doi.org/10.1016/S0734-189X(86)80031-7, URL http://www.sciencedirect.com/science/article/pii/S0734189X86800317.

[19] WhiteTimberwolf, "Schematic drawing of an octree," https://commons.wikimedia.org/w/index.php?curid=9851485, Mar. 2010. (Accessed on 03/01/2018).

[20] Edelsbrunner, H., Kirkpatrick, D., and Seidel, R., "On the Shape of a Set of Points in the Plane," *IEEE Transactions on Information Theory*, Vol. 29, No. 4, 1983, pp. 551–559. doi:10.1109/TIT.1983.1056714.

[21] Ostro, S. J., and Benner, L. A. M., "Asteroid Shape Model - NASA JPL," https://echo.jpl.nasa.gov/asteroids/shapes/shapes.html, Dec 2008. (Accessed on 10/01/2018).